

Observation of two charged bottomonium-like resonances

I. Adachi,¹³ K. Adamczyk,⁴⁴ H. Aihara,⁶⁸ K. Arinstein,^{2,48} Y. Arita,³⁸ D. M. Asner,⁵¹
T. Aso,⁷² V. Aulchenko,^{2,48} T. Aushev,^{32,24} T. Aziz,⁶³ A. M. Bakich,⁶² V. Balagura,²⁴
Y. Ban,⁵³ E. Barberio,³⁷ A. Bay,³² I. Bedny,^{2,48} M. Belhorn,⁵ K. Belous,²¹ V. Bhardwaj,⁵²
B. Bhuyan,¹⁶ M. Bischofberger,⁴⁰ S. Blyth,⁴² A. Bondar,^{2,48} G. Bonvicini,⁷⁴ A. Bozek,⁴⁴
M. Bračko,^{35,25} J. Brodzicka,⁴⁴ O. Brovchenko,²⁷ T. E. Browder,¹² M.-C. Chang,⁶
P. Chang,⁴³ Y. Chao,⁴³ A. Chen,⁴¹ K.-F. Chen,⁴³ P. Chen,⁴³ B. G. Cheon,¹¹ R. Chistov,²⁴
I.-S. Cho,⁷⁶ K. Cho,²⁸ K.-S. Choi,⁷⁶ S.-K. Choi,¹⁰ Y. Choi,⁶¹ J. Crnkovic,¹⁵ J. Dalseno,^{36,64}
M. Danilov,²⁴ A. Das,⁶³ Z. Doležal,³ Z. Drásal,³ A. Drutskoy,⁵ Y.-T. Duh,⁴³ W. Dungel,²⁰
D. Dutta,¹⁶ S. Eidelman,^{2,48} D. Epifanov,^{2,48} S. Esen,⁵ J. E. Fast,⁵¹ M. Feindt,²⁷
M. Fujikawa,⁴⁰ V. Gaur,⁶³ N. Gabyshev,^{2,48} A. Garmash,^{2,48} Y. M. Goh,¹¹ B. Golob,^{33,25}
M. Grosse Perdekamp,^{15,56} H. Guo,⁵⁸ H. Ha,²⁹ J. Haba,¹³ Y. L. Han,¹⁹ K. Hara,³⁸
T. Hara,¹³ Y. Hasegawa,⁶⁰ K. Hayasaka,³⁸ H. Hayashii,⁴⁰ D. Heffernan,⁵⁰ T. Higuchi,¹³
C.-T. Hoi,⁴³ Y. Horii,⁶⁷ Y. Hoshi,⁶⁶ K. Hoshina,⁷¹ W.-S. Hou,⁴³ Y. B. Hsiung,⁴³ C.-L. Hsu,⁴³
H. J. Hyun,³¹ Y. Igarashi,¹³ T. Iijima,³⁸ M. Imamura,³⁸ K. Inami,³⁸ A. Ishikawa,⁵⁷
R. Itoh,¹³ M. Iwabuchi,⁷⁶ M. Iwasaki,⁶⁸ Y. Iwasaki,¹³ T. Iwashita,⁴⁰ S. Iwata,⁷⁰ I. Jaegle,¹²
M. Jones,¹² N. J. Joshi,⁶³ T. Julius,³⁷ H. Kakuno,⁶⁸ J. H. Kang,⁷⁶ P. Kapusta,⁴⁴
S. U. Kataoka,³⁹ N. Katayama,¹³ H. Kawai,⁴ T. Kawasaki,⁴⁶ H. Kichimi,¹³ C. Kiesling,³⁶
H. J. Kim,³¹ H. O. Kim,³¹ J. B. Kim,²⁹ J. H. Kim,²⁸ K. T. Kim,²⁹ M. J. Kim,³¹
S. H. Kim,¹¹ S. H. Kim,²⁹ S. K. Kim,⁵⁹ T. Y. Kim,¹¹ Y. J. Kim,²⁸ K. Kinoshita,⁵
B. R. Ko,²⁹ N. Kobayashi,^{55,69} S. Koblitz,³⁶ P. Kodyš,³ Y. Koga,³⁸ S. Korpar,^{35,25}
R. T. Kouzes,⁵¹ M. Kreps,²⁷ P. Križan,^{33,25} T. Kuhr,²⁷ R. Kumar,⁵² T. Kumita,⁷⁰
E. Kurihara,⁴ Y. Kuroki,⁵⁰ A. Kuzmin,^{2,48} P. Kvasnička,³ Y.-J. Kwon,⁷⁶ S.-H. Kyeong,⁷⁶
J. S. Lange,⁷ I. S. Lee,¹¹ M. J. Lee,⁵⁹ S. E. Lee,⁵⁹ S.-H. Lee,²⁹ M. Leitgab,^{15,56} R. Leitner,³
J. Li,⁵⁹ Y. Li,⁷³ J. Libby,¹⁷ C.-L. Lim,⁷⁶ A. Limosani,³⁷ C. Liu,⁵⁸ Y. Liu,⁴³ Z. Q. Liu,¹⁹
D. Liventsev,²⁴ R. Louvot,³² J. MacNaughton,¹³ D. Marlow,⁵⁴ A. Matyjka,⁴⁴ S. McOnie,⁶²
T. Medvedeva,²⁴ Y. Mikami,⁶⁷ M. Nayak,¹⁷ K. Miyabayashi,⁴⁰ Y. Miyachi,^{55,75}
H. Miyata,⁴⁶ Y. Miyazaki,³⁸ R. Mizuk,²⁴ G. B. Mohanty,⁶³ D. Mohapatra,⁷³ A. Moll,^{36,64}
T. Mori,³⁸ T. Müller,²⁷ N. Muramatsu,^{55,50} R. Mussa,²³ T. Nagamine,⁶⁷ Y. Nagasaka,¹⁴
Y. Nakahama,⁶⁸ I. Nakamura,¹³ E. Nakano,⁴⁹ T. Nakano,^{55,50} M. Nakao,¹³ H. Nakayama,¹³

H. Nakazawa,⁴¹ Z. Natkaniec,⁴⁴ E. Nedelkovska,³⁶ K. Neichi,⁶⁶ S. Neubauer,²⁷ C. Ng,⁶⁸
M. Niiyama,^{55,30} S. Nishida,¹³ K. Nishimura,¹² O. Nitoh,⁷¹ S. Noguchi,⁴⁰ T. Nozaki,¹³
A. Ogawa,⁵⁶ S. Ogawa,⁶⁵ T. Ohshima,³⁸ S. Okuno,²⁶ S. L. Olsen,^{59,12} Y. Onuki,⁶⁷
W. Ostrowicz,⁴⁴ H. Ozaki,¹³ P. Pakhlov,²⁴ G. Pakhlova,²⁴ H. Palka,⁴⁴ C. W. Park,⁶¹
H. Park,³¹ H. K. Park,³¹ K. S. Park,⁶¹ L. S. Peak,⁶² T. K. Pedlar,³⁴ T. Peng,⁵⁸
R. Pestotnik,²⁵ M. Peters,¹² M. Petrič,²⁵ L. E. Piilonen,⁷³ A. Poluektov,^{2,48} M. Prim,²⁷
K. Prothmann,^{36,64} B. Reisert,³⁶ M. Ritter,³⁶ M. Röhrken,²⁷ J. Rorie,¹² M. Rozanska,⁴⁴
S. Ryu,⁵⁹ H. Sahoo,¹² K. Sakai,¹³ Y. Sakai,¹³ D. Santel,⁵ N. Sasao,³⁰ O. Schneider,³²
P. Schönmeier,⁶⁷ C. Schwanda,²⁰ A. J. Schwartz,⁵ R. Seidl,⁵⁶ A. Sekiya,⁴⁰ K. Senyo,³⁸
O. Seon,³⁸ M. E. Seviar,³⁷ L. Shang,¹⁹ M. Shapkin,²¹ V. Shebalin,^{2,48} C. P. Shen,¹²
T.-A. Shibata,^{55,69} H. Shibuya,⁶⁵ S. Shinomiya,⁵⁰ J.-G. Shiu,⁴³ B. Shwartz,^{2,48}
F. Simon,^{36,64} J. B. Singh,⁵² R. Sinha,²² P. Smerkol,²⁵ Y.-S. Sohn,⁷⁶ A. Sokolov,²¹
E. Solovieva,²⁴ S. Stanič,⁴⁷ M. Starič,²⁵ J. Stypula,⁴⁴ S. Sugihara,⁶⁸ A. Sugiyama,⁵⁷
M. Sumihama,^{55,8} K. Sumisawa,¹³ T. Sumiyoshi,⁷⁰ K. Suzuki,³⁸ S. Suzuki,⁵⁷ S. Y. Suzuki,¹³
H. Takeichi,³⁸ M. Tanaka,¹³ S. Tanaka,¹³ N. Taniguchi,¹³ G. Tatishvili,⁵¹ G. N. Taylor,³⁷
Y. Teramoto,⁴⁹ I. Tikhomirov,²⁴ K. Trabelsi,¹³ Y. F. Tse,³⁷ T. Tsuboyama,¹³ Y.-W. Tung,⁴³
M. Uchida,^{55,69} T. Uchida,¹³ Y. Uchida,⁹ S. Uehara,¹³ K. Ueno,⁴³ T. Uglov,²⁴ M. Ullrich,⁷
Y. Unno,¹¹ S. Uno,¹³ P. Urquijo,¹ Y. Ushiroda,¹³ Y. Usov,^{2,48} S. E. Vahsen,¹²
P. Vanhoefer,³⁶ G. Varner,¹² K. E. Varvell,⁶² K. Vervink,³² A. Vinokurova,^{2,48} A. Vossen,¹⁸
C. H. Wang,⁴² J. Wang,⁵³ M.-Z. Wang,⁴³ P. Wang,¹⁹ X. L. Wang,¹⁹ M. Watanabe,⁴⁶
Y. Watanabe,²⁶ R. Wedd,³⁷ M. Werner,⁷ E. White,⁵ J. Wicht,¹³ L. Widhalm,²⁰
J. Wiechczynski,⁴⁴ K. M. Williams,⁷³ E. Won,²⁹ T.-Y. Wu,⁴³ B. D. Yabsley,⁶²
H. Yamamoto,⁶⁷ J. Yamaoka,¹² Y. Yamashita,⁴⁵ M. Yamauchi,¹³ C. Z. Yuan,¹⁹ Y. Yusa,⁷³
D. Zander,²⁷ C. C. Zhang,¹⁹ L. M. Zhang,⁵⁸ Z. P. Zhang,⁵⁸ L. Zhao,⁵⁸ V. Zhilich,^{2,48}
P. Zhou,⁷⁴ V. Zhulanov,^{2,48} T. Zivko,²⁵ A. Zupanc,²⁷ N. Zwahlen,³² and O. Zyukova^{2,48}

(The Belle Collaboration)

¹*University of Bonn, Bonn*

²*Budker Institute of Nuclear Physics, Novosibirsk*

³*Faculty of Mathematics and Physics, Charles University, Prague*

⁴*Chiba University, Chiba*

- ⁵*University of Cincinnati, Cincinnati, Ohio 45221*
- ⁶*Department of Physics, Fu Jen Catholic University, Taipei*
- ⁷*Justus-Liebig-Universität Gießen, Gießen*
- ⁸*Gifu University, Gifu*
- ⁹*The Graduate University for Advanced Studies, Hayama*
- ¹⁰*Gyeongsang National University, Chinju*
- ¹¹*Hanyang University, Seoul*
- ¹²*University of Hawaii, Honolulu, Hawaii 96822*
- ¹³*High Energy Accelerator Research Organization (KEK), Tsukuba*
- ¹⁴*Hiroshima Institute of Technology, Hiroshima*
- ¹⁵*University of Illinois at Urbana-Champaign, Urbana, Illinois 61801*
- ¹⁶*Indian Institute of Technology Guwahati, Guwahati*
- ¹⁷*Indian Institute of Technology Madras, Madras*
- ¹⁸*Indiana University, Bloomington, Indiana 47408*
- ¹⁹*Institute of High Energy Physics,
Chinese Academy of Sciences, Beijing*
- ²⁰*Institute of High Energy Physics, Vienna*
- ²¹*Institute of High Energy Physics, Protvino*
- ²²*Institute of Mathematical Sciences, Chennai*
- ²³*INFN - Sezione di Torino, Torino*
- ²⁴*Institute for Theoretical and Experimental Physics, Moscow*
- ²⁵*J. Stefan Institute, Ljubljana*
- ²⁶*Kanagawa University, Yokohama*
- ²⁷*Institut für Experimentelle Kernphysik,
Karlsruher Institut für Technologie, Karlsruhe*
- ²⁸*Korea Institute of Science and Technology Information, Daejeon*
- ²⁹*Korea University, Seoul*
- ³⁰*Kyoto University, Kyoto*
- ³¹*Kyungpook National University, Taegu*
- ³²*École Polytechnique Fédérale de Lausanne (EPFL), Lausanne*
- ³³*Faculty of Mathematics and Physics, University of Ljubljana, Ljubljana*
- ³⁴*Luther College, Decorah, Iowa 52101*

- ³⁵*University of Maribor, Maribor*
- ³⁶*Max-Planck-Institut für Physik, München*
- ³⁷*University of Melbourne, School of Physics, Victoria 3010*
- ³⁸*Nagoya University, Nagoya*
- ³⁹*Nara University of Education, Nara*
- ⁴⁰*Nara Women's University, Nara*
- ⁴¹*National Central University, Chung-li*
- ⁴²*National United University, Miao Li*
- ⁴³*Department of Physics, National Taiwan University, Taipei*
- ⁴⁴*H. Niewodniczanski Institute of Nuclear Physics, Krakow*
- ⁴⁵*Nippon Dental University, Niigata*
- ⁴⁶*Niigata University, Niigata*
- ⁴⁷*University of Nova Gorica, Nova Gorica*
- ⁴⁸*Novosibirsk State University, Novosibirsk*
- ⁴⁹*Osaka City University, Osaka*
- ⁵⁰*Osaka University, Osaka*
- ⁵¹*Pacific Northwest National Laboratory, Richland, Washington 99352*
- ⁵²*Panjab University, Chandigarh*
- ⁵³*Peking University, Beijing*
- ⁵⁴*Princeton University, Princeton, New Jersey 08544*
- ⁵⁵*Research Center for Nuclear Physics, Osaka*
- ⁵⁶*RIKEN BNL Research Center, Upton, New York 11973*
- ⁵⁷*Saga University, Saga*
- ⁵⁸*University of Science and Technology of China, Hefei*
- ⁵⁹*Seoul National University, Seoul*
- ⁶⁰*Shinshu University, Nagano*
- ⁶¹*Sungkyunkwan University, Suwon*
- ⁶²*School of Physics, University of Sydney, NSW 2006*
- ⁶³*Tata Institute of Fundamental Research, Mumbai*
- ⁶⁴*Excellence Cluster Universe, Technische Universität München, Garching*
- ⁶⁵*Toho University, Funabashi*
- ⁶⁶*Tohoku Gakuin University, Tagajo*

⁶⁷*Tohoku University, Sendai*

⁶⁸*Department of Physics, University of Tokyo, Tokyo*

⁶⁹*Tokyo Institute of Technology, Tokyo*

⁷⁰*Tokyo Metropolitan University, Tokyo*

⁷¹*Tokyo University of Agriculture and Technology, Tokyo*

⁷²*Toyama National College of Maritime Technology, Toyama*

⁷³*CNP, Virginia Polytechnic Institute and State University, Blacksburg, Virginia 24061*

⁷⁴*Wayne State University, Detroit, Michigan 48202*

⁷⁵*Yamagata University, Yamagata*

⁷⁶*Yonsei University, Seoul*

(Dated: November 7, 2018)

Abstract

We report the observation of two narrow structures at $10610 \text{ MeV}/c^2$ and $10650 \text{ MeV}/c^2$ in the $\pi^\pm \Upsilon(nS)$ ($n = 1, 2, 3$) and $\pi^\pm h_b(mP)$ ($m = 1, 2$) mass spectra that are produced in association with a single charged pion in $\Upsilon(5S)$ decays. The measured masses and widths of the two structures averaged over the five final states are $M_1 = 10608.4 \pm 2.0 \text{ MeV}/c^2$, $\Gamma_1 = 15.6 \pm 2.5 \text{ MeV}$ and $M_2 = 10653.2 \pm 1.5 \text{ MeV}/c^2$, $\Gamma_2 = 14.4 \pm 3.2 \text{ MeV}$. Analysis favors quantum numbers of $I^G(J^P) = 1^+(1^+)$ for both states. The results are obtained with a 121.4 fb^{-1} data sample collected with the Belle detector near the $\Upsilon(5S)$ resonance at the KEKB asymmetric-energy e^+e^- collider.

PACS numbers: 14.40.Pq, 13.25.Gv, 12.39.Pn

INTRODUCTION

Analyses of decays of the $\Upsilon(5S)$ resonance to non- $B_s\bar{B}_s$ final states have produced several surprises. Recently the Belle Collaboration reported observation of anomalously high rates for $\Upsilon(5S) \rightarrow \Upsilon(nS)\pi^+\pi^-$ ($n = 1, 2, 3$) [1] and $\Upsilon(5S) \rightarrow h_b(mP)\pi^+\pi^-$ ($m = 1, 2$) [2] transitions. If the $\Upsilon(nS)$ signals are attributed entirely to $\Upsilon(5S)$ decays, the measured partial decay widths $\Gamma[\Upsilon(5S) \rightarrow \Upsilon(nS)\pi^+\pi^-] \sim 0.5 \text{ MeV}$ are about two orders of magnitude larger than typical widths for dipion transitions among the four lower $\Upsilon(nS)$ states. The rates for the $\Upsilon(5S) \rightarrow h_b(mP)\pi^+\pi^-$ transitions are found to be comparable with those for $\Upsilon(5S) \rightarrow \Upsilon(nS)\pi^+\pi^-$, indicating that processes requiring a heavy-quark spin flip - i.e., in $h_b(mP)$ production - do not seem to be suppressed. These unexpected observations indicate that exotic mechanisms could be contributing to the $\Upsilon(5S)$ decays.

We report preliminary results of detailed studies of the three-body $\Upsilon(5S) \rightarrow \Upsilon(nS)\pi^+\pi^-$ ($n = 1, 2, 3$) and $\Upsilon(5S) \rightarrow h_b(mP)\pi^+\pi^-$ ($m = 1, 2$) decays. Results are obtained with a 121.4 fb^{-1} data sample collected near the peak of the $\Upsilon(5S)$ resonance ($\sqrt{s} \sim 10.865 \text{ GeV}$) with the Belle detector at the KEKB asymmetric energy e^+e^- collider [3].

BELLE DETECTOR

The Belle detector is a large-solid-angle magnetic spectrometer that consists of a 4-layer silicon vertex detector (SVD), a 50-layer central drift chamber (CDC), an array of aerogel threshold Cherenkov counters (ACC), a barrel-like arrangement of time-of-flight scintillation counters (TOF), and an electromagnetic calorimeter (ECL) comprising CsI(Tl) crystals located inside a superconducting solenoid coil that provides a 1.5 T magnetic field. An iron flux-return located outside of the coil is instrumented to detect K_L^0 mesons and to identify muons (KLM). The detector is described in detail elsewhere [4].

For charged hadron identification, the dE/dx measurement in the CDC and the response of the ACC and TOF are combined to form a single likelihood ratio. Electron identification is based on a combination of dE/dx measurement, the response of the ACC, and the position, shape and total energy deposition of the shower detected in the ECL. Muons are identified by their range and transverse scattering in the KLM.

We use a GEANT-based Monte Carlo (MC) simulation [5] to model the response of the

detector and determine the acceptance. The MC simulation includes run-dependent detector performance variations and background conditions.

ANALYSIS OF $\Upsilon(5S) \rightarrow \Upsilon(1S, 2S, 3S)\pi^+\pi^-$

To select $\Upsilon(5S) \rightarrow \Upsilon(nS)\pi^+\pi^-$ candidate events we require the presence of a pair of muon candidates with an invariant mass in the range of $8.0 \text{ GeV}/c^2 < M(\mu^+\mu^-) < 11.0 \text{ GeV}/c^2$ and two pion candidates of opposite charge. These tracks are required to be consistent with coming from the interaction point: we apply requirements $dr < 0.5 \text{ cm}$ and $|dz| < 2.5 \text{ cm}$, where dr and $|dz|$ are impact parameters perpendicular to and along the beam axis with respect to the interaction point, respectively. We also require that none of the four tracks is positively identified as an electron. No additional requirements are applied at this stage.

Candidate $\Upsilon(5S) \rightarrow \Upsilon(nS)\pi^+\pi^-$ events are identified by the invariant mass of the $\mu^+\mu^-$ combination and the missing mass $MM(\pi^+\pi^-)$ associated with the $\pi^+\pi^-$ system calculated as

$$MM(\pi^+\pi^-) = \sqrt{(E_{c.m.} - E_{\pi^+\pi^-}^*)^2 - p_{\pi^+\pi^-}^{*2}}, \quad (1)$$

where $E_{c.m.}$ is the center-of-mass (c.m.) energy and $E_{\pi^+\pi^-}^*$ and $p_{\pi^+\pi^-}^*$ are the energy and momentum of the $\pi^+\pi^-$ system measured in the c.m. frame. The two-dimensional distribution of $M(\mu^+\mu^-)$ versus $MM(\pi^+\pi^-)$ for all the preselected candidates is shown in Fig. 1. Events originated from $\Upsilon(5S)$ decay fall within the narrow diagonal band ($\Upsilon(5S)$ signal region) defined as $|MM(\pi^+\pi^-) - M(\mu^+\mu^-)| < 0.2 \text{ GeV}/c^2$ (see Fig. 1). Clustering of events around nominal $\Upsilon(nS)$ mass values [6] are clearly visible on the plot.

The amplitude analyses of the three-body $\Upsilon(5S) \rightarrow \Upsilon(nS)\pi^+\pi^-$ decays that are reported here are performed by means of unbinned maximum likelihood fits to two-dimensional Dalitz distributions.

Before fitting the Dalitz plot for events in the signal region, we determine the distribution of background events over the Dalitz plot using events in the $\Upsilon(nS)$ mass sidebands that are refitted to the nominal mass of the corresponding $\Upsilon(nS)$ state to match the phase space boundaries. Definitions of the mass sidebands are given in Table I and the corresponding sideband Dalitz plots are shown in Fig. 2, where $M(\Upsilon(nS)\pi)_{\min}$ and $M(\Upsilon(nS)\pi)_{\max}$ are defined as $M(\Upsilon(nS)\pi)_{\min} = \min(M(\Upsilon(nS)\pi^+), M(\Upsilon(nS)\pi^-))$ and $M(\Upsilon(nS)\pi)_{\max} = \max(M(\Upsilon(nS)\pi^+), M(\Upsilon(nS)\pi^-))$, respectively.

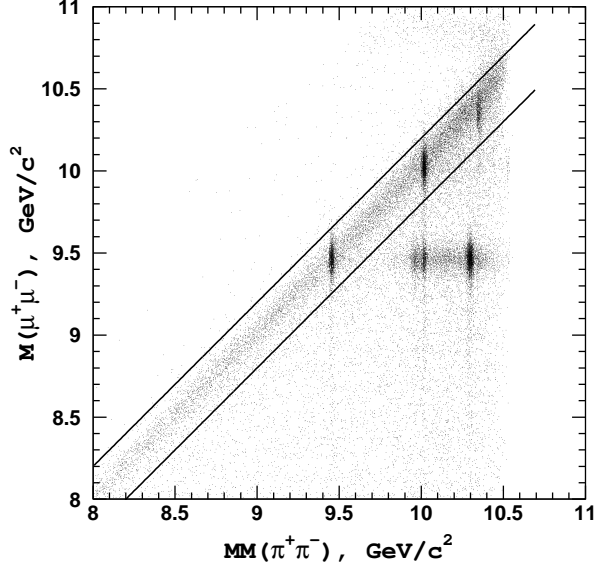


FIG. 1: A scatter plot of all of the $\Upsilon(5S) \rightarrow \Upsilon(nS)\pi^+\pi^-$ candidate events that pass the initial selection criteria. The area between the two diagonal lines is the $\Upsilon(5S)$ signal region.

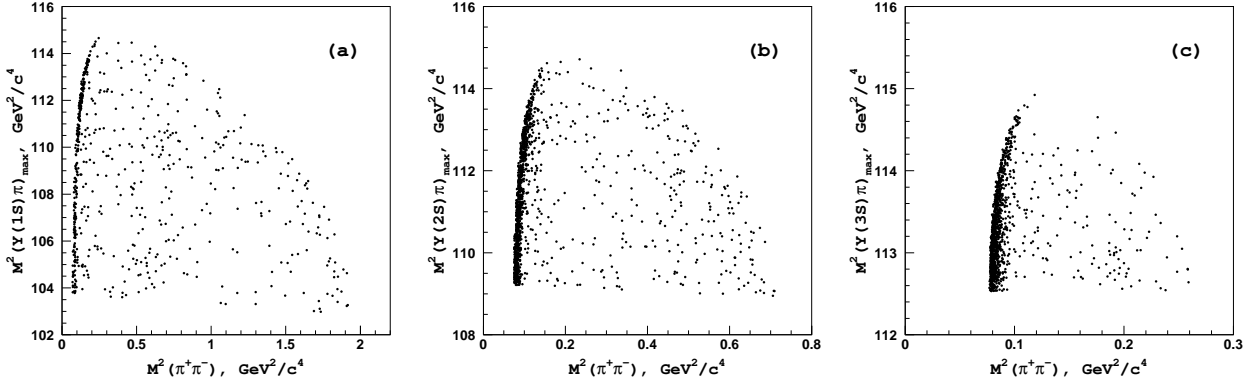


FIG. 2: Dalitz plots for $\Upsilon(nS)\pi^+\pi^-$ events in the (a) $\Upsilon(1S)$; (b) $\Upsilon(2S)$; (c) $\Upsilon(3S)$ sidebands.

It is evident in the sideband Dalitz distributions, shown in Fig. 2, that there is a strong

TABLE I: Definition of the sidebands for $\Upsilon(nS)\pi^+\pi^-$ signals. The sidebands are defined in terms of regions in the spectrum of the missing mass associated with the $\pi^+\pi^-$ system.

Final state	$\Upsilon(1S)\pi^+\pi^-$	$\Upsilon(2S)\pi^+\pi^-$	$\Upsilon(3S)\pi^+\pi^-$
Sideband region, GeV/c^2	$9.38 < MM(\pi\pi) < 9.43$ $9.48 < MM(\pi\pi) < 9.53$	$9.95 < MM(\pi\pi) < 10.00$ $10.05 < MM(\pi\pi) < 10.10$	$10.28 < MM(\pi\pi) < 10.33$ $10.38 < MM(\pi\pi) < 10.43$

concentration of background events in the very low $\pi^+\pi^-$ invariant mass region; these are due to photon conversion in the innermost parts of the Belle detector. Because of their low energy, these conversion electrons are poorly identified and pass the electron veto requirement. We exclude this high background region by applying the requirements on the $\pi^+\pi^-$ invariant mass given in Table II. For the remainder of the Dalitz plot the distribution of background events is assumed to be uniform. The variation of reconstruction efficiency across the Dalitz plot is determined from MC simulation. The fraction of signal events in the signal region for each of the three $\Upsilon(nS)\pi^+\pi^-$ final states is determined from a fit to the corresponding $MM(\pi^+\pi^-)$ spectrum using a Crystal Ball function [7] for the Υ signal and a linear function for the combinatorial background component. Results of the fits are shown in Fig. 3 and are summarized in Table II.

Figure 4 shows Dalitz plots of the events in the signal regions for the three decay channels under study. In all cases, two horizontal bands are evident in the $\Upsilon(nS)\pi$ system near $10.61 \text{ GeV}/c^2$ ($\sim 112.6 \text{ GeV}^2/c^4$) and $10.65 \text{ GeV}/c^2$ ($\sim 113.3 \text{ GeV}^2/c^4$). In the following we refer to these structures as $Z_b(10610)$ and $Z_b(10650)$, respectively.

We use the following parameterization for the $\Upsilon(5S) \rightarrow \Upsilon(nS)\pi^+\pi^-$ three-body decay amplitude:

$$M(s_1, s_2) = A_1(s_1, s_2) + A_2(s_1, s_2) + A_{f_0} + A_{f_2} + A_{NR}, \quad (2)$$

TABLE II: Results of the fits to the $MM(\pi^+\pi^-)$ missing mass distributions.

Final state	$\Upsilon(1S)\pi^+\pi^-$	$\Upsilon(2S)\pi^+\pi^-$	$\Upsilon(3S)\pi^+\pi^-$
$M(\pi^+\pi^-)$ signal region, GeV/c^2	$0.20 < M(\pi^+\pi^-)$	$0.16 < M(\pi^+\pi^-)$	$0.10 < M(\pi^+\pi^-)$
$MM(\pi^+\pi^-)$ signal region, GeV/c^2	$9.43 < MM(\pi^+\pi^-)$ $MM(\pi^+\pi^-) < 9.48$	$10.00 < MM(\pi^+\pi^-)$ $MM(\pi^+\pi^-) < 10.05$	$10.33 < MM(\pi^+\pi^-)$ $MM(\pi^+\pi^-) < 10.38$
Peak position, GeV/c^2	9455.3 ± 1.1	10019.1 ± 1.7	10350.2 ± 2.3
Resolution, MeV/c^2	7.31	6.74	6.33
Number of events	1581	1926	689
Signal fraction	0.902 ± 0.015	0.937 ± 0.007	0.917 ± 0.010

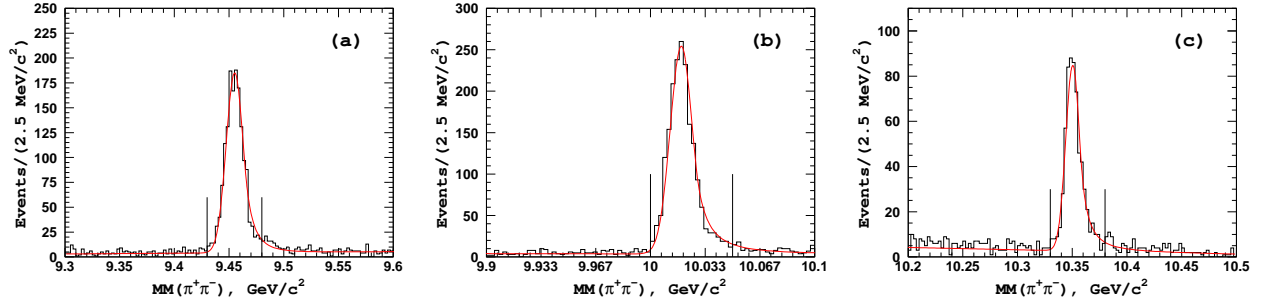


FIG. 3: Distribution of missing mass associated with the $\pi^+\pi^-$ combination for $\Upsilon(5S) \rightarrow \Upsilon(nS)\pi^+\pi^-$ candidate events in the (a) $\Upsilon(1S)$; (b) $\Upsilon(2S)$; (c) $\Upsilon(3S)$ mass regions. Vertical lines define the corresponding signal regions.

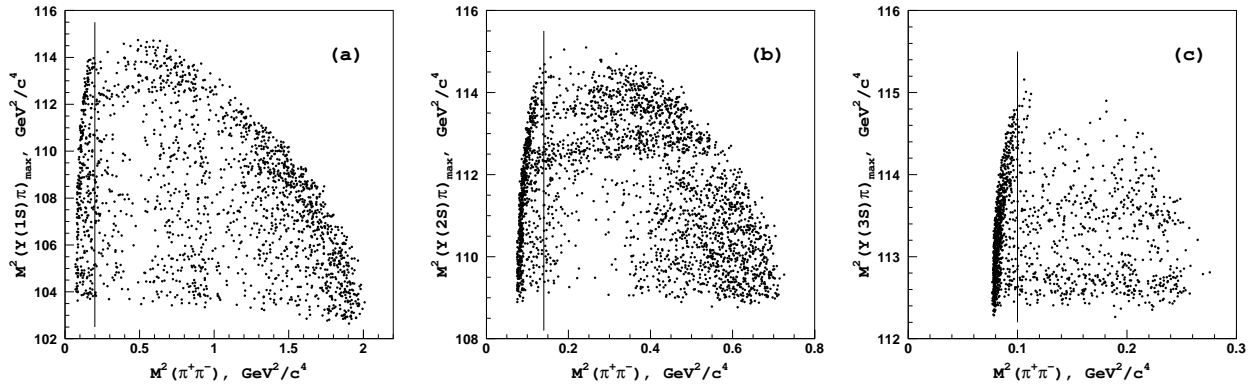


FIG. 4: Dalitz plots for $\Upsilon(nS)\pi^+\pi^-$ events in the (a) $\Upsilon(1S)$; (b) $\Upsilon(2S)$; (c) $\Upsilon(3S)$ signal regions. Dalitz plot regions to the right of the vertical lines are included in the amplitude analysis.

where $s_1 = M^2(\Upsilon(nS)\pi^+)$, $s_2 = M^2(\Upsilon(nS)\pi^-)$. Here we assume that the dominant contributions come from amplitudes that conserve the orientation of the spin of the heavy quarkonium state and, thus, both pions in the cascade decay $\Upsilon(5S) \rightarrow Z_b\pi \rightarrow \Upsilon(nS)\pi^+\pi^-$ are emitted in an S -wave with respect to the heavy quarkonium system. As will be shown later, angular analyses support this assumption. Consequently, we parameterize the observed $Z_b(10610)$ and $Z_b(10650)$ peaks with an S -wave Breit-Wigner function

$$BW(s, M, \Gamma) = \frac{\Gamma}{M^2 - s - iM\Gamma}, \quad (3)$$

where we do not consider possible s -dependence of the resonance width Γ . To account for the possibility of $\Upsilon(5S)$ decay to both $Z^+\pi^-$ and $Z^-\pi^+$, the amplitudes A_1 and A_2 are symmetrized with respect to π^+ and π^- transposition. Taking into account isospin

symmetry, the resulting amplitude is written as

$$A_k(s_1, s_2) = a_k e^{i\delta_k} (BW(s_1, M_k, \Gamma_k) + BW(s_2, M_k, \Gamma_k)), \quad (4)$$

where the masses M_k and the widths Γ_k ($k = 1, 2$) are free parameters of the fit. Due to the very limited phase space available in the $\Upsilon(5S) \rightarrow \Upsilon(3S)\pi^+\pi^-$ decay, there is a significant overlap between the two processes $\Upsilon(5S) \rightarrow Z_b^+\pi^-$ and $\Upsilon(5S) \rightarrow Z_b^-\pi^+$. We also include A_{f_0} and A_{f_2} amplitudes to account for possible contributions in the $\pi^+\pi^-$ channel from $f_0(980)$ scalar and $f_2(1270)$ tensor states, respectively. Inclusion of the $f_0(980)$ state is necessary in order to describe the prominent structure in the $M(\pi^+\pi^-)$ spectrum for the $\Upsilon(1S)\pi^+\pi^-$ final state around $M(\pi^+\pi^-) = 1.0 \text{ GeV}/c^2$ (see Fig. 5). We also find that the addition of the $f_2(1270)$ gives a better description of the data at $M(\pi^+\pi^-) > 1.0 \text{ GeV}/c^2$ and drastically improves the fit likelihood values. We use a Breit-Wigner function to parameterize the $f_2(1270)$ and a coupled-channel Breit-Wigner (Flatte) function [8] for the $f_0(980)$. The mass and the width of the $f_2(1270)$ state are fixed at their world average values [6]; the mass and the coupling constants of the $f_0(980)$ state are fixed at values defined from the analysis of $B^+ \rightarrow K^+\pi^+\pi^-$: $M(f_0(980)) = 950 \text{ MeV}/c^2$, $g_{\pi\pi} = 0.23$, $g_{KK} = 0.73$ [9].

Following suggestions given in Refs.[10] and references therein, the non-resonant amplitude A_{NR} has been parameterized as

$$A_{NR} = a_1^{\text{nr}} e^{i\delta_1^{\text{nr}}} + a_2^{\text{nr}} e^{i\delta_2^{\text{nr}}} s_3, \quad (5)$$

where $s_3 = M^2(\pi^+\pi^-)$ (s_3 is not an independent variable and can be expressed via s_1 and s_2 but we use it here for clarity), a_1^{nr} , a_2^{nr} , δ_1^{nr} and δ_2^{nr} are free parameters of the fit (with an exceptions of the $\Upsilon(3S)\pi^+\pi^-$ channel as described below).

The logarithmic likelihood function \mathcal{L} is then constructed as

$$\mathcal{L} = -2 \sum \log(f_{\text{sig}} S(s_1, s_2) + (1 - f_{\text{sig}}) B(s_1, s_2)), \quad (6)$$

where $S(s_1, s_2) = |M(s_1, s_2)|^2$ folded with the detector resolution function ($2 \text{ MeV}/c^2$ for $M(\Upsilon(nS)\pi^\pm)$ when both $\Upsilon(nS)$ and $\Upsilon(5S)$ mass constraints are used; the $M(\pi^+\pi^-)$ resolution is not taken into account since no narrow resonances are observed in the $\pi^+\pi^-$ system), $B(s_1, s_2) = 1$ and f_{sig} is a fraction of signal events in the data sample. Both $S(s_1, s_2)$ and $B(s_1, s_2)$ are corrected for reconstruction efficiency.

In the fit to the $\Upsilon(1S)\pi^+\pi^-$ sample, the amplitudes and phases of all of the components are allowed to float. However, in the $\Upsilon(2S)\pi^+\pi^-$ and $\Upsilon(3S)\pi^+\pi^-$ samples the available

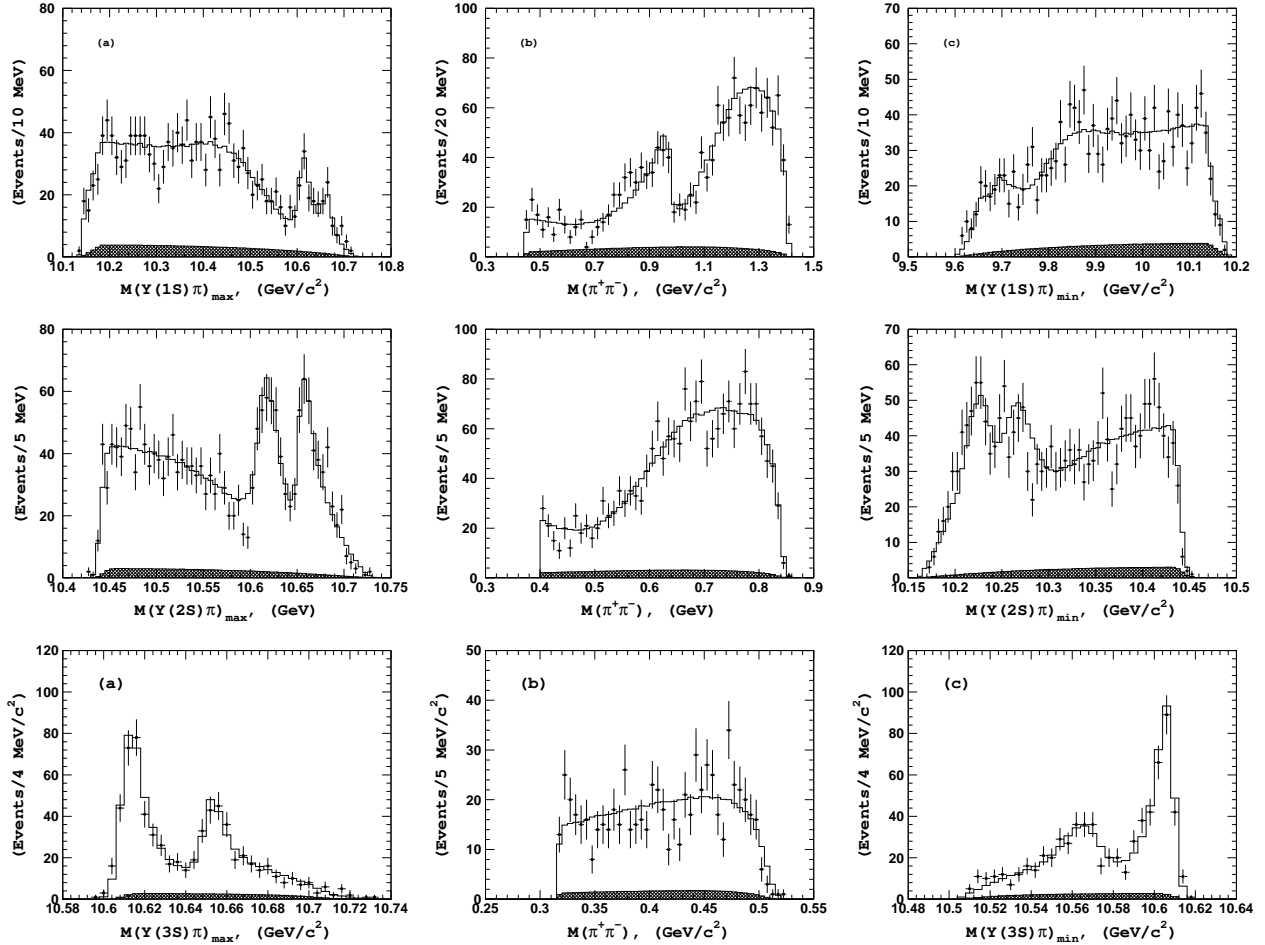


FIG. 5: Comparison of fit results (open histogram) with experimental data (points with error bars) for events in the $\Upsilon(1S)$ (top row), $\Upsilon(2S)$ (middle row), and $\Upsilon(3S)$ (bottom top) signal regions. The hatched histogram show the background component.

phase space is significantly smaller and contributions from the $f_0(980)$ and $f_2(1270)$ are not well defined. Thus, in the fit to the $\Upsilon(2S)\pi^+\pi^-$ and $\Upsilon(3S)\pi^+\pi^-$ signal samples, we fix the amplitudes and relative phases of these components to the values measured in the fit to the $\Upsilon(1S)\pi^+\pi^-$ sample. Moreover, in the fit to the $\Upsilon(3S)\pi^+\pi^-$ sample, we also fix the a_2^{nr} and δ_2^{nr} parameters of the A_{nr} amplitude. Possible effects of these assumptions are considered while determining the model-dependent uncertainty. Results of the fits to $\Upsilon(5S) \rightarrow \Upsilon(nS)\pi^+\pi^-$ signal events are shown in Fig. 5, where one-dimensional projections of the data and fits are compared. To combine Z_b^+ and Z_b^- events we plot $\Upsilon(nS)\pi$ mass distributions in terms of $M(\Upsilon(nS)\pi)_{\text{min}}$ and $M(\Upsilon(nS)\pi)_{\text{max}}$; fits are performed in terms of $M(\Upsilon(nS)\pi^+)$ and $M(\Upsilon(nS)\pi^-)$. Results of the fits are summarized in Table VI. We try various alternative

models to parameterize the decay amplitude as described in the systematic uncertainty section. The combined statistical significance of the two peaks exceeds 10σ for all tested models and for all $\Upsilon(nS)\pi^+\pi^-$ channels.

The main sources of systematic uncertainties are found to be:

- Dependence of reconstruction efficiency on the Dalitz plot variables has been determined from MC simulation of signal events uniformly distributed over the Dalitz plot. Since the pions from the $\Upsilon(5S) \rightarrow \Upsilon(nS)\pi^+\pi^-$ decays have low momenta, the efficiency determined from MC might be systematically shifted by up to 5-10%. The effect on the parameters of the observed peaks is estimated by varying the efficiency at the edges of the Dalitz plot by $\pm 10\%$ and refitting the data.
- To estimate the effect of the parameterization used to fit the data on the parameters of the Z_b peaks we fit the data with modifications of the nominal model described in Eq. 2. In particular, we vary the $M(\pi^+\pi^-)$ dependence of the non-resonant amplitude A_{NR} , try to include a D -wave component into A_{NR} , etc. The variations in the extracted Z_b parameters determined from fits with modified models are taken as estimates of the model uncertainties.
- The uncertainty in the c.m. energy leads to an uncertainty in Dalitz plot boundaries. This effect is particularly important for the $\Upsilon(3S)\pi^+\pi^-$ channel. To estimate the associated effect on the Z_b parameters, we generate normalization phase space MC samples that correspond to $E_{c.m.} \pm 3$ MeV, where $E_{c.m.}$ is the nominal c.m. energy.

Systematic effects associated with uncertainties in the description of the combinatorial background is found to be negligible. The results of our studies on systematic uncertainties are summarized in Table III.

ANALYSIS OF $\Upsilon(5S) \rightarrow h_b(1P, 2P)\pi^+\pi^-$

$h_b(1P)$ and $h_b(2P)$ have been recently observed by Belle in the decay $\Upsilon(5S) \rightarrow h_b(mP)\pi^+\pi^-$ [2]. Here we study resonant structure of these decays. Because of high background Dalitz plot analysis is impossible with current statistics, therefore we study the one dimensional distributions in $M(h_b(mP)\pi)$. We use the same selection requirements and reconstruction procedure as in Ref. [2].

TABLE III: Summary of dominant sources of systematic uncertainties. Uncertainties for masses and widths are given in MeV/ c^2 and in degrees for the relative phase. Quoted numbers are for $\Upsilon(1S)/\Upsilon(2S)/\Upsilon(3S)$ channels, respectively.

Parameter	Efficiency	Model	$E_{c.m.}$	Total
$M(Z_b(10610))$	$\pm 1/\pm 1/\pm 1$	$\pm 1/_{-3}^{+2}/_{-0}^{+4}$	$\pm 1/\pm 1/\pm 2$	$\pm 2/_{-4}^{+3}/_{-2}^{+5}$
$\Gamma(Z_b(10610))$	$\pm 1/\pm 1/\pm 1$	$\pm 2/_{-1.4}^{+0.3}/_{1.2}^{+2.4}$	$\pm 1/\pm 2/\pm 3$	$\pm 2/_{-3}^{+2}/\pm 4$
$M(Z_b(10650))$	$\pm 1/\pm 1/\pm 1$	$\pm 1/_{-1}^{+1}/_{-1}^{+2}$	$\pm 1/\pm 1/\pm 1$	$\pm 2/\pm 2/\pm 2$
$\Gamma(Z_b(10650))$	$\pm 1/\pm 1/\pm 1$	$\pm 2/_{-4.6}^{+1.4}/_{-0.2}^{+3.7}$	$\pm 1/\pm 3/\pm 1$	$\pm 3/_{-6}^{+4}/_{-2}^{+4}$
Rel. phase	$\pm 3/_{-4}^{+6}/\pm 5$	$_{-50}^{+0}/_{-6}^{+11}/_{-58}^{+21}$	$\pm 3/\pm 6/\pm 9$	$_{-50}^{+5}/_{-9}^{+14}/_{-59}^{+23}$
Rel. amp.	$\pm 0.01/ \pm 0.02/ \pm 0.02$	$_{-0.0}^{+0.08}/_{-0.0}^{+0.03}/_{-0.02}^{+0.14}$	$\pm 0.02/ \pm 0.02/ \pm 0.04$	$_{-0.03}^{+0.09}/_{-0.03}^{+0.04}/_{-0.05}^{+0.15}$

The $\Upsilon(5S) \rightarrow h_b(mP)\pi^+\pi^-$ decays are reconstructed inclusively using the missing mass of the $\pi^+\pi^-$ pair. We select π^+ and π^- candidates that originate from the vicinity of the interaction point ($dr < 3$ mm, $|dz| < 2$ cm) and are positively identified as pions. We reject tracks that are identified as electrons. The continuum $e^+e^- \rightarrow q\bar{q}$ ($q = u, d, s, c$) background is suppressed by a requirement on the ratio of the second to zeroth Fox-Wolfram moments $R_2 < 0.3$ [11].

We define the $M(h_b(mP)\pi^+)$ as a missing mass of the opposite sign pion, $MM(\pi^-)$. We measure the yield of signal decays as a function of the $MM(\pi^\pm)$ by fitting the $MM(\pi^+\pi^-)$ spectra in the bins of $MM(\pi^\pm)$. We combine the $MM(\pi^+\pi^-)$ spectra for the corresponding $MM(\pi^+)$ and $MM(\pi^-)$ bins and we use half of the phase-space to avoid double counting, as shown in Fig. 6.

In the studies of the $\Upsilon(5S) \rightarrow h_b(1P)\pi^+\pi^-$ channel we subdivide the interval $10.4 \text{ MeV}/c^2 < MM(\pi) < 10.72 \text{ MeV}/c^2$ into 32 bins and perform a χ^2 fit to the $MM(\pi^+\pi^-)$ spectrum for each $MM(\pi)$ bin. The fit function consists of four components: the $h_b(1P)$ signal, the $\Upsilon(2S)$ signal, a reflection from the $\Upsilon(3S) \rightarrow \Upsilon(1S)\pi^+\pi^-$ decay, and combinatorial background. The shapes of the signal components and $\Upsilon(3S)$ reflection is determined from the analysis of exclusive $\mu^+\mu^-\pi^+\pi^-$ data as described in Ref. [2]. The signals are parameterized by a Crystal Ball function to accommodate tails due to initial state radiation of soft photons that accounts for about 8% of the signal yield. The resolution width of the

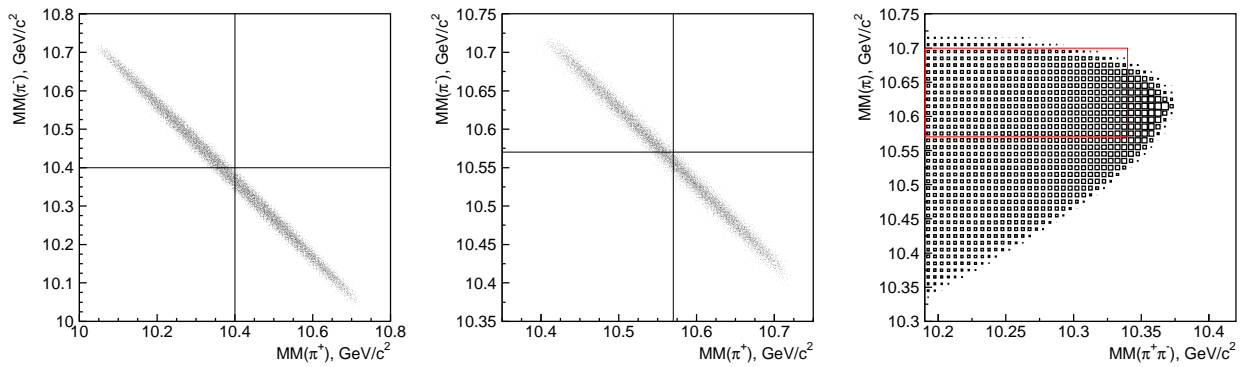


FIG. 6: The $MM(\pi^-)$ versus $MM(\pi^+)$ distribution for the $\Upsilon(5S) \rightarrow h_b(1P)\pi^+\pi^-$ (left) and $\Upsilon(5S) \rightarrow h_b(2P)\pi^+\pi^-$ (middle) events simulated according to the phase-space MC model. Lines indicate the values of cuts used to avoid double counting after symmetrization relative to π^+ and π^- . Right: the $MM(\pi)$ versus $MM(\pi^+\pi^-)$ distribution for inclusive $K_S^0 \rightarrow \pi^+\pi^-$ signal in the fast MC simulation. The red rectangle shows the fit region for the $h_b(2P)\pi^+\pi^-$ analysis.

$\Upsilon(2S)$ ($h_b(1P)$) is $\sigma = 6.5 \text{ MeV}/c^2$ ($6.8 \text{ MeV}/c^2$). The $\Upsilon(3S) \rightarrow \Upsilon(1S)\pi^+\pi^-$ reflection is described by a single Gaussian function with the width of $\sigma = 18 \text{ MeV}$. The ratio of the $\Upsilon(3S) \rightarrow \Upsilon(1S)\pi^+\pi^-$ and $\Upsilon(2S)$ yields is measured from $\mu^+\mu^-\pi^+\pi^-$ data and corrected for the branching fractions for $\Upsilon(1S) \rightarrow \mu^+\mu^-$ and $\Upsilon(2S) \rightarrow \mu^+\mu^-$ decays. In the fit to the inclusive $MM(\pi^+\pi^-)$ spectra, this ratio is allowed to float within the uncertainties of the exclusive $\mu^+\mu^-\pi^+\pi^-$ measurements. The combinatorial background is parameterized by a Chebyshev polynomial. The polynomial order decreases monotonically from 10-th order for the first bin to 6-th order for the 11-th bin. The background shape in the first $MM(\pi)$ bins is complicated due to the proximity of the kinematic boundary, therefore a high-order polynomial is used.

Results of fits for the $h_b(1P)$ and $\Upsilon(2S)$ yield as a function of $MM(\pi)$ are shown in Fig. 7, where the $\Upsilon(2S)$ yield measured from the analysis of the exclusive $\Upsilon(5S) \rightarrow \mu^+\mu^-\pi^+\pi^-$ data and renormalized to the total number of events in inclusive spectrum is also shown for comparison. The $\Upsilon(2S)$ yields for inclusive and exclusive measurements agree well. The $h_b(1P)$ yield shown in Fig. 7 exhibits a clear two-peak structure without any significant non-resonant contribution. The peak positions are consistent with those for the $Z_b(10610)$ and $Z_b(10650)$ observed in the $\Upsilon(nS)\pi^\pm$ final states.

We perform a χ^2 fit to the $MM(\pi)$ distribution. We assume that spin-parity for both

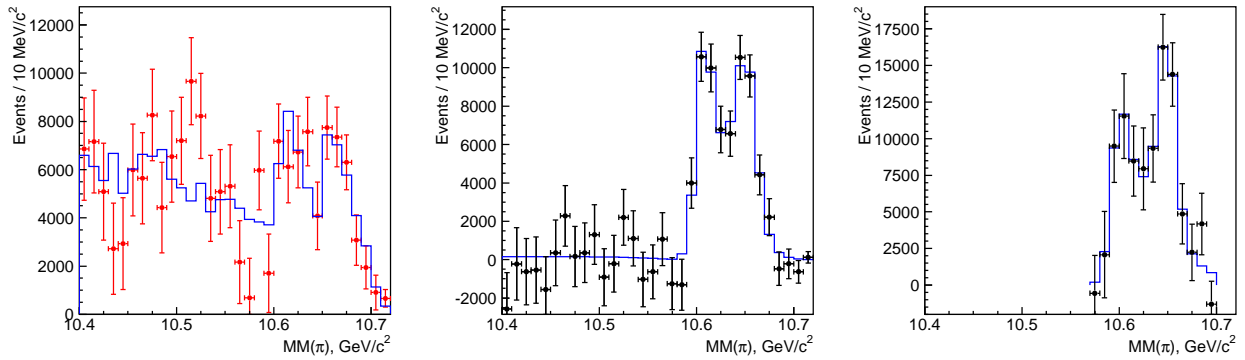


FIG. 7: Left: the yield of $\Upsilon(2S)$ as a function of the $MM(\pi)$ measured using the inclusive data (points with error bars) and exclusive $\mu^+\mu^-\pi^+\pi^-$ data (histogram). Middle: the yield of the $h_b(1P)$ as a function of $MM(\pi)$ (points with error bars) and results of the fit (histogram). Right: the yield of the $h_b(2P)$ as a function of $MM(\pi)$ (points with error bars) and results of the fit (histogram).

$Z_b(10610)$ and $Z_b(10650)$ is $J^P = 1^+$, therefore in the fit function we use a coherent sum of two P -wave Breit-Wigner amplitudes; we add also a non-resonant contribution.

$$f = A |BW(s, M_1, \Gamma_1) + ae^{i\phi} BW(s, M_2, \Gamma_2) + be^{i\psi}|^2 \frac{qp}{\sqrt{s}}. \quad (7)$$

Here $\sqrt{s} \equiv MM(\pi)$; the variables A , M_k , Γ_k ($k = 1, 2$), a , ϕ , b and ψ are floating in the fit; $\frac{qp}{\sqrt{s}}$ is a phase-space factor, p (q) is the momentum of the pion originating from the $\Upsilon(5S)$ (Z_b) decay measured in the rest frame of the corresponding mother particle.

The P -wave Breit-Wigner amplitude is expressed as

$$BW(s, M, \Gamma) = \frac{q/\sqrt{s} F}{M^2 - s - iM\Gamma(s)}. \quad (8)$$

Here F is the P -wave Blatt-Weisskopf form-factor $F = \sqrt{\frac{1+(q_0R)^2}{1+(qR)^2}}$ [12], q_0 is daughter momentum calculated assuming pole mass of its mother, $R = 1.6 \text{ GeV}^{-1}$; $\Gamma(s)$ is the energy-dependent width, $\Gamma(s) = \Gamma(\frac{q}{q_0})^3 \frac{M}{\sqrt{s}} F^2$. The function f is convolved with the detector resolution function, is integrated over the $10 \text{ MeV}/c^2$ wide bin and is corrected for reconstruction efficiency. The detector resolution is parameterized by a single Gaussian function with $\sigma = 5.2 \text{ MeV}/c^2$ as determined from MC simulation. The result of the fit is shown in Fig. 7 and is summarized in Table VI. The non-resonant amplitude is found to be consistent with zero, $b = 0.03 \pm 0.04$. The confidence level of the fit is 81%. We find that the hypothesis of

two resonances is favored over the hypothesis of a single resonance (no resonances) at the 7.4σ (17.9σ) level.

The systematic uncertainty is estimated by varying (within ± 2) the order of the Chebyshev polynomial and repeating the fit to the data. We also perform fits with the constraint on the normalization of the $\Upsilon(3S) \rightarrow \Upsilon(1S)\pi^+\pi^-$ reflection released. We shift the $MM(\pi)$ binning by half the bin-size. To estimate the uncertainty due to fit model, we try to fit the $MM(\pi)$ spectrum with the non-resonant component fixed at zero. We vary the Blatt-Weisskopf parameter R from 0 to 5 GeV^{-1} . As found in Ref. [2], the detector resolution as determined from a MC simulation could be underestimated by as much as 5-10%. To account for this effect we repeat the fit to the $MM(\pi)$ spectrum with a corrected resolution function. The maximal change of signal parameters for each source is considered as a systematic uncertainty. We find that the systematic uncertainties associated with releasing the constraint on the $\Upsilon(3S) \rightarrow \Upsilon(1S)\pi^+\pi^-$ reflection and varying R are negligible. Finally, we find about $1\text{ MeV}/c^2$ deviations of the $\Upsilon(1S)$, $\Upsilon(2S)$ and $\Upsilon(3S)$ peak positions relative to the PDG values when the $\Upsilon(nS)$ states are reconstructed inclusively [2]. These small deviations could be due to the local variations of the background shape that are not fully described by the polynomial. Consequently, we add an additional uncertainty of $1\text{ MeV}/c^2$ to all mass measurements. All contributions are added in quadrature to obtain the total systematic uncertainty. The summary of systematic uncertainties study is presented in Table IV. The minimal level at which the two-resonance hypothesis is favored over the one-resonance (no-resonance) hypothesis for all considered variations is 6.6σ (16.0σ).

The analysis of the $h_b(2P)\pi^+\pi^-$ final state follows the same strategy as that for the $h_b(1P)\pi^+\pi^-$. In this case we require $MM(\pi) > 10.57\text{ GeV}/c^2$ to avoid double counting of signal events. We also require $MM(\pi^+\pi^-) < 10.34\text{ GeV}/c^2$ and $MM(\pi) < 10.7\text{ GeV}/c^2$ to minimize influence of the reflections from events where the two charged pions originate from a $K_S^0 \rightarrow \pi^+\pi^-$ decay (see Fig. 6). We subdivide the interval $10.57\text{ GeV}/c^2 < MM(\pi) < 10.7\text{ GeV}/c^2$ into 13 bins and perform χ^2 fits to the $MM(\pi^+\pi^-)$ spectra for each $MM(\pi)$ bin. The fit function consists of three components: the $h_b(2P)$ signal, reflection from the $\Upsilon(2S) \rightarrow \Upsilon(1S)\pi^+\pi^-$ decay and combinatorial background. The $\Upsilon(3S)$ signal is outside the mass range. The shapes of the signal and reflection are determined from the analysis of the exclusive $\Upsilon(5S) \rightarrow \mu^+\mu^-\pi^+\pi^-$ data. The yield of the reflection for each $MM(\pi)$ bin is determined from the exclusive $\mu^+\mu^-\pi^+\pi^-$ data and is normalized to the ratio of inclusive

TABLE IV: Systematic uncertainties in the mass and width of the $Z_b(10610)$ (index 1) and $Z_b(10650)$ (index 2), their relative normalization factor a and phase ϕ for the $h_b(1P)\pi^+\pi^-/h_b(2P)\pi^+\pi^-$ decay modes.

	Chebyshev polynomial order	$MM(\pi)$ binning	Fit model	Resolution	Total
$M_1, \text{ MeV}/c^2$	+2.6/+4 -0/-1	+0.1/+0 -0/-2	+1.1/+3 -0/-0	+0.3/+0 -0/-0	+3.0/+5 -1.0/-2
$\Gamma_1, \text{ MeV}$	+1.5/+9 -0/-3	+1.4/+10 -0/-0	+0.1/+0 -0/-3	+0/+0 -1.2/-1	+2.1/+13 -1.2/-4
$M_2, \text{ MeV}/c^2$	+0/+1 -0.4/-2	+0/+2 -0.6/-0	+0/+0 -1.4/-0	+0/+0 -0.3/-0	+1.0/+2 -1.9/-2
$\Gamma_2, \text{ MeV}$	+0/+2 -5.5/-2	+2.1/+4 -0/-0	+0/+7 -0.2/-0	+0/+0 -0.8/-1	+2.1/+8 -5.7/-2
a	+0.1/+0.2 -0.5/-0.7	+0/+0 -0/-0.1	+0/+0.4 -0.1/-0	+0/+0 -0/-0	+0.1/+0.4 -0.5/-0.7
$\phi, \text{ degree}$	+4/+11 -4/-167	+0/+5 -2/-0	+0/+0 -8/-74	+0/+0 -1/-0	+4/+12 -9/-193

and exclusive yields. The systematic uncertainty in the inclusive yield estimated in Ref. [2] is taken into account. When fitting the inclusive $MM(\pi^+\pi^-)$ spectra in bins of $MM(\pi)$ we allow the yield of the reflection to float within the uncertainty of the above measurement. Combinatorial background is parameterized by a Chebyshev polynomial function. The order of the polynomial varies from 6 to 8 for different $MM(\pi)$ bins. The fit results for the $h_b(2P)$ yield is presented in Fig. 7.

To fit the $MM(\pi)$ distribution of the $h_b(2P)$ signal we use the same fit function as for the $h_b(1P)$. The result of the fit is shown in Fig. 7. As in the case of the $h_b(1P)$, the non-resonant amplitude is found to be consistent with zero, 0.11 ± 0.13 . Numerical values for other parameters are given in Table VI. The confidence level of the fit is 42%. The two-resonance hypothesis is favored over that for one resonance (no resonances) at the 2.7σ (6.3σ) level.

The systematic uncertainty is estimated in the same way as for the $h_b(1P)$, the results are given in Table IV. The minimal level at which the two-resonance hypothesis is favored over the one-resonance (no-resonance) one for all considered variations is 1.9σ (4.7σ).

ANGULAR ANALYSIS

We perform angular analyses to check consistency of the $J^P = 1^+$ assignment for the $Z_b(10610)$ and $Z_b(10650)$ states and to attempt to discriminate against other J^P hypotheses; we consider $J^P = 1^-, 2^+$ and 2^- . The 0^+ (0^-) assignment is forbidden by parity conservation in $Z_b \rightarrow \Upsilon(nS)\pi$ ($Z_b \rightarrow h_b(mP)\pi$) decays. We use the polar angles of the pions (denoted as θ_1 for a pion from the $Y(5S)$ decay and θ_2 for a pion from the Z_b decay), the spatial angle, $\theta_{\pi\pi}$, between the two pions and the angle, ϕ_p , between the plane defined by the pion from $Y(5S)$ decay and the beam direction and the plane defined by the two pions. Since the Z_b velocity is very small, $\beta < 0.02$, we neglect its recoil motion and measure all pion momenta in the c.m. frame. We assume that only the lowest partial wave contributes to the decay in the cases where more than one partial wave is possible [13].

$\Upsilon(2S)\pi^+\pi^-$ and $\Upsilon(3S)\pi^+\pi^-$ final states

We apply an additional requirement on the angle between the two pion momenta measured in the laboratory frame, $\cos\theta_{\text{lab}} < 0.95$, to suppress the background from converted photons.

We first study the angular distribution for the non-resonant component for the $\Upsilon(2S)\pi^+\pi^-$ candidates. The non-resonant region is defined as $10.5 \text{ GeV}/c^2 < M(\Upsilon\pi) < 10.58 \text{ GeV}/c^2$. The $\cos\theta_{\pi\pi}$ values is tightly correlated with the $M(\pi^+\pi^-)$, therefore the $\cos\theta_{\pi\pi}$ distribution reflects the details of the $M(\pi^+\pi^-)$ distribution discussed in the Dalitz analysis section of the paper. The $\cos\theta_1$, $\cos\theta_2$ and ϕ_p distributions (after the $MM(\pi^+\pi^-)$ sideband subtraction and efficiency correction) are all consistent with uniform distributions. This indicates that the non-resonant contribution is dominated by an S -wave component.

At the next step we select the $Z_b(10610)$ [$Z_b(10650)$] region $10.602 < M(\Upsilon(2S)\pi) < 10.638 \text{ GeV}/c^2$ [$10.648 < M(\Upsilon(2S)\pi) < 10.7 \text{ GeV}/c^2$] for the $\Upsilon(2S)\pi^+\pi^-$ final state and $10.607 < M(\Upsilon(3S)\pi) < 10.627 \text{ GeV}/c^2$ [$10.649 < M(\Upsilon(2S)\pi) < 10.676 \text{ GeV}/c^2$] for the $\Upsilon(3S)\pi^+\pi^-$ final state. For the $\Upsilon(2S)\pi^+\pi^-$ candidates we require $0.15 \text{ GeV}^2/c^4 < M^2(\pi^+\pi^-) < 0.4 \text{ GeV}^2/c^4$, which considerably suppresses the non-resonant contribution. The $\cos\theta_1$, $\cos\theta_2$ and ϕ_p distributions corrected for the reconstruction efficiency are shown in Figs 8 and 9.

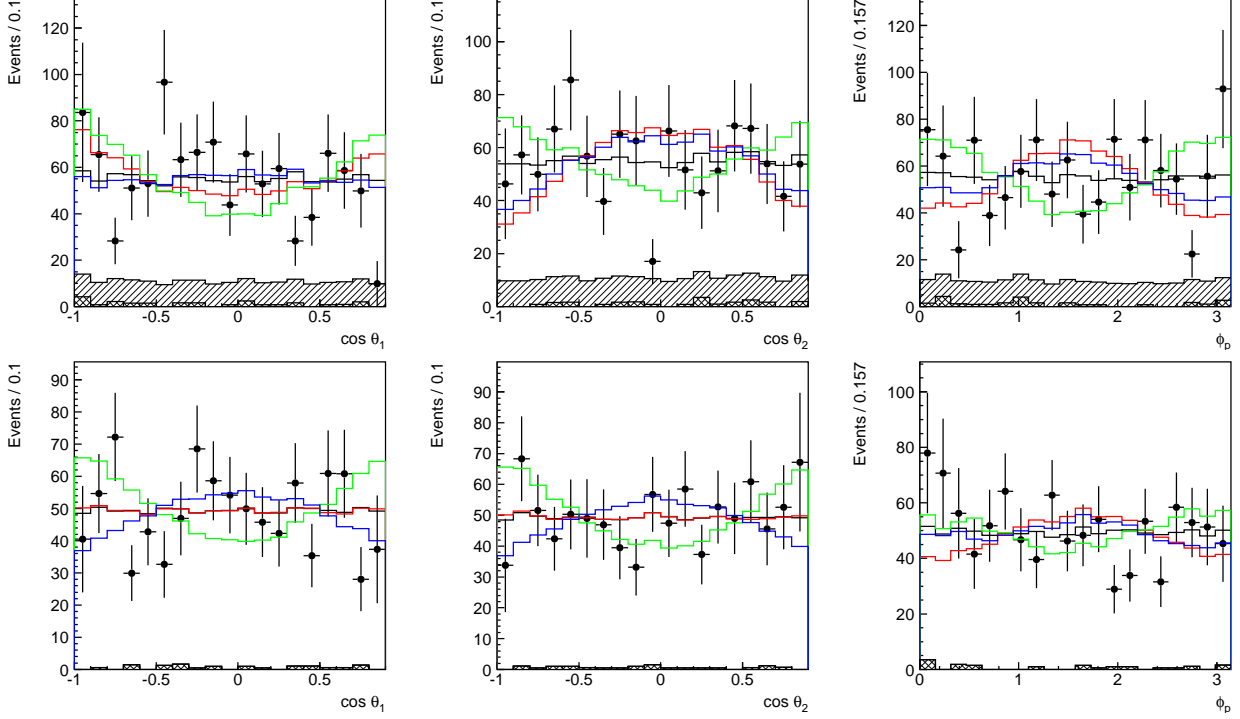


FIG. 8: Angular distributions for the $Z_b(10610)$ signal region. Points with error bars represent the yield of the $\Upsilon(2S)\pi$ candidates (first row) and $\Upsilon(3S)\pi$ candidates (second row) as a function of the $\cos\theta_1$ (left column), $\cos\theta_2$ (middle column) and ϕ_p (right column). The open histograms represent the fit results for different J^P hypotheses: 1^+ (black), 1^- (red), 2^+ (green) and 2^- (blue). The hatched (cross-hatched) histogram shows the contribution of the non-resonant (combinatorial) component.

We perform a binned maximum likelihood fit to these distributions. The fit function is a sum of three components: (a) the Z_b signal, (b) the contribution due to the non-resonant component and (c) combinatorial background described by a properly normalized $MM(\pi^+\pi^-)$ sidebands. The terms due to the interference of the Z_b signal and S -wave non-resonant part are constant in $\cos\theta_1$, $\cos\theta_2$ and ϕ_p . Therefore, component (b) of the fit function is a constant. We estimate its normalization from the linear extrapolation in the $M(\Upsilon(2S)\pi)$ for the $\Upsilon(2S)\pi^+\pi^-$ final state and we assume that it is zero for the $\Upsilon(3S)\pi^+\pi^-$ final state. The non-resonant contribution varies with $\cos\theta_{\pi\pi}$, therefore this variable is not used. The components (a) and (b) of the fit function are corrected for efficiency. The only floating parameter in the fit is the normalization of the Z_b signal component [14].

The fit results for various Z_b spin-parity assignments are shown in Figs. 8 and 9. We use

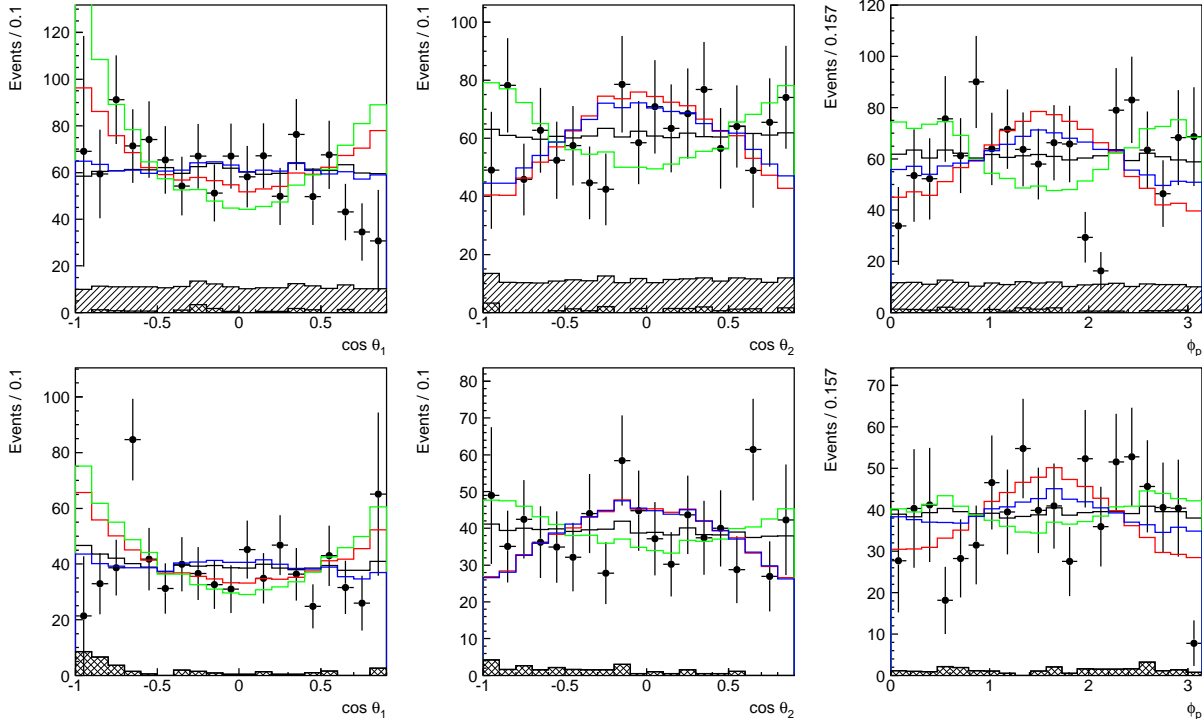


FIG. 9: Angular distributions for the $Z_b(10650)$ signal region. The histogram contents are similar to those shown in Fig. 8.

$\cos \theta_2$ to discriminate 1^+ from 1^- and 1^+ from 2^- , and we use $\cos \theta_1$ to discriminate 1^+ from 2^+ . The probabilities at which the 1^- , 2^+ and 2^- hypotheses are disfavored compared to the 1^+ hypothesis are calculated as $\sqrt{\Delta 2 \log L}$ and given in Table V.

TABLE V: The probabilities at which different J^P hypotheses are disfavored compared to the 1^+ hypothesis. The data are consistent with the 1^+ hypothesis.

J^P	$Z_b(10610)$			$Z_b(10650)$		
	$\Upsilon(2S)\pi^+\pi^-$	$\Upsilon(3S)\pi^+\pi^-$	$h_b(1P)\pi^+\pi^-$	$\Upsilon(2S)\pi^+\pi^-$	$\Upsilon(3S)\pi^+\pi^-$	$h_b(1P)\pi^+\pi^-$
1^-	3.6σ	0.3σ	0.3σ	3.7σ	2.6σ	2.7σ
2^+	4.3σ	3.5σ	4.3σ	4.4σ	2.7σ	2.1σ
2^-	2.7σ	2.8σ		2.9σ	2.6σ	

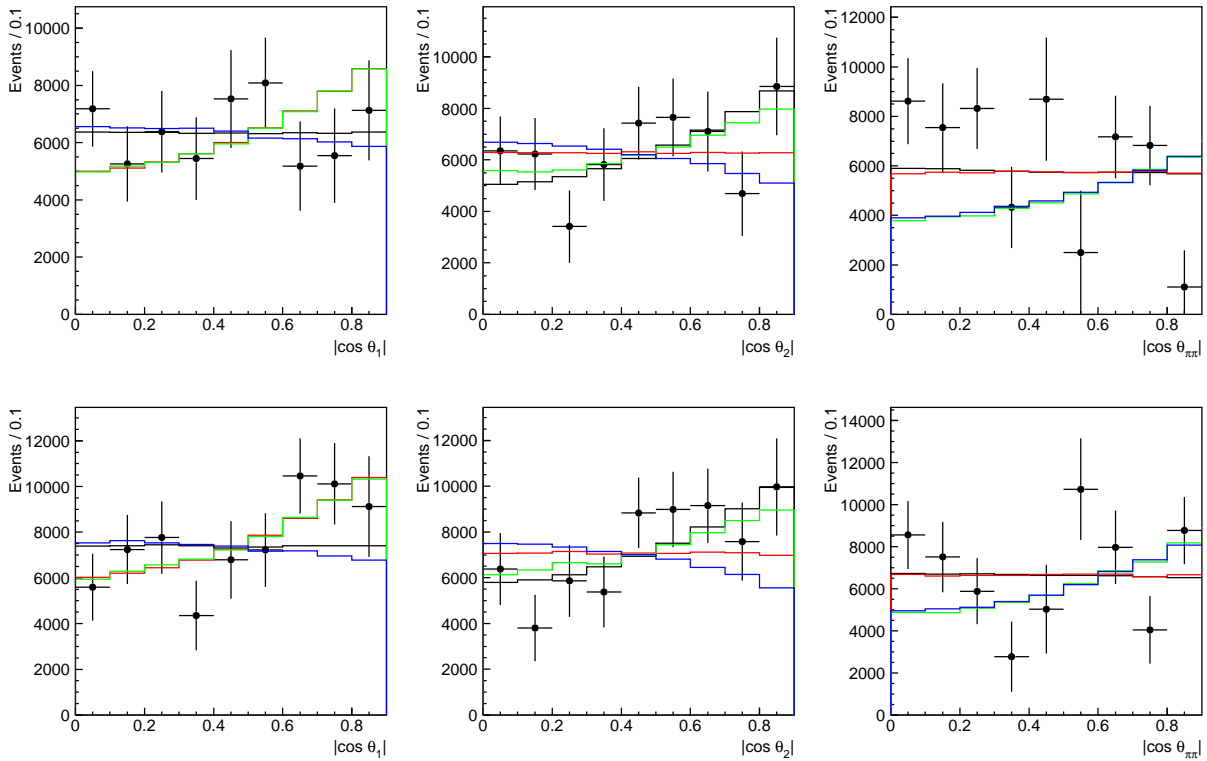


FIG. 10: Points with error bars represent the $h_b(1P)$ yield as a function of the $\cos \theta_1$ (left column), $\cos \theta_2$ (middle column) and $\cos \theta_{\pi\pi}$ (right column) for the $Z_b(10610)$ (top row) and $Z_b(10650)$ (bottom row) regions. Histograms represent the fit results for different J^P hypotheses: 1^+ (black), 1^- (red), 2^+ (green) and 2^- (blue).

$h_b(1P)\pi^+\pi^-$ final state

We define the $Z_b(10610)$ and $Z_b(10650)$ signal regions as $10.6 \text{ GeV}/c^2 < MM(\pi) < 10.63 \text{ GeV}/c^2$ and $10.63 \text{ GeV}/c^2 < MM(\pi) < 10.67 \text{ GeV}/c^2$, respectively. For each region we fit the $MM(\pi^+\pi^-)$ spectra in bins of $\cos \theta_1$, $\cos \theta_2$ and $\cos \theta_{\pi\pi}$ to determine the $h_b(1P)$ signal yield. The $h_b(1P)$ yield corrected for the reconstruction efficiency as a function of angular variables is shown in Fig 10. The results of the fits to the different spin-parity hypotheses are superimposed. We use $\cos \theta_{\pi\pi}$ to discriminate 1^+ from 2^+ and 1^+ from 2^- , and we use $\cos \theta_2$ to discriminate 1^+ from 1^- . The level at which the 1^- , 2^+ and 2^- hypotheses are disfavored compared to the 1^+ hypothesis is calculated as a square root of the difference of the corresponding χ^2 values and is shown in Table V.

The values quoted in Table V are preliminary. Our procedure to deal with the non-

TABLE VI: Comparison of results on $Z_b(10610)$ and $Z_b(10650)$ parameters obtained from $\Upsilon(5S) \rightarrow \Upsilon(nS)\pi^+\pi^-$ ($n = 1, 2, 3$) and $\Upsilon(5S) \rightarrow h_b(mP)\pi^+\pi^-$ ($m = 1, 2$) analyses. Quoted values are in MeV/ c^2 for masses, in MeV for widths and in degrees for the relative phase. Relative amplitude is defined as $a_{Z_b(10650)}/a_{Z_b(10610)}$.

Final state	$\Upsilon(1S)\pi^+\pi^-$	$\Upsilon(2S)\pi^+\pi^-$	$\Upsilon(3S)\pi^+\pi^-$	$h_b(1P)\pi^+\pi^-$	$h_b(2P)\pi^+\pi^-$
$M(Z_b(10610))$	$10609 \pm 3 \pm 2$	$10616 \pm 2^{+3}_{-4}$	$10608 \pm 2^{+5}_{-2}$	$10605.1 \pm 2.2^{+3.0}_{-1.0}$	$10596 \pm 7^{+5}_{-2}$
$\Gamma(Z_b(10610))$	$22.9 \pm 7.3 \pm 2$	$21.1 \pm 4^{+2}_{-3}$	$12.2 \pm 1.7 \pm 4$	$11.4^{+4.5+2.1}_{-3.9-1.2}$	16^{+16+13}_{-10-4}
$M(Z_b(10650))$	$10660 \pm 6 \pm 2$	$10653 \pm 2 \pm 2$	$10652 \pm 2 \pm 2$	$10654.5 \pm 2.5^{+1.0}_{-1.9}$	$10651 \pm 4 \pm 2$
$\Gamma(Z_b(10650))$	$12 \pm 10 \pm 3$	$16.4 \pm 3.6^{+4}_{-6}$	$10.9 \pm 2.6^{+4}_{-2}$	$20.9^{+5.4+2.1}_{-4.7-5.7}$	12^{+11+8}_{-9-2}
Rel. amplitude	$0.59 \pm 0.19^{+0.09}_{-0.03}$	$0.91 \pm 0.11^{+0.04}_{-0.03}$	$0.73 \pm 0.10^{+0.15}_{-0.05}$	$1.8^{+1.0+0.1}_{-0.7-0.5}$	$1.3^{+3.1+0.4}_{-1.1-0.7}$
Rel. phase,	$53 \pm 61^{+5}_{-50}$	$-20 \pm 18^{+14}_{-9}$	$6 \pm 24^{+23}_{-59}$	188^{+44+4}_{-58-9}	$255^{+56+12}_{-72-183}$

resonant contribution is approximate, and we do not take into account mutual cross-feed of the $Z_b(10610)$ and $Z_b(10650)$ states. However, the angular analyses indicate that the 1^+ hypothesis for both $Z_b(10610)$ and $Z_b(10650)$ provides the best description of angular distributions compared to all other hypotheses with $J \leq 2$.

DISCUSSION AND CONCLUSIONS

In conclusion, we have observed two charged bottomonium-like resonances, the $Z_b(10610)$ and $Z_b(10650)$, with signals in five different decay channels, $\Upsilon(nS)\pi^\pm$ ($n = 1, 2, 3$) and $h_b(mP)\pi^\pm$ ($m = 1, 2$). Parameters of the resonances as measured in different channels are summarized in Table VI. All channels yield consistent results as can be seen in Fig. 11. A simple weighted averages over all five channels give $M[Z_b(10610)] = 10608.4 \pm 2.0$ MeV/ c^2 , $\Gamma[Z_b(10610)] = 15.6 \pm 2.5$ MeV and $M[Z_b(10650)] = 10653.2 \pm 1.5$ MeV/ c^2 , $\Gamma[Z_b(10650)] = 14.4 \pm 3.2$ MeV, where statistical and systematic errors are added in quadrature.

Charged bottomonium-like resonances cannot be simple $b\bar{b}$ combinations. The measured masses of these new states exceed by only a few MeV/ c^2 the thresholds for the open beauty channels $B^*\bar{B}$ (10604.6 MeV) and $B^*\bar{B}^*$ (10650.2 MeV). This ‘‘coincidence’’ is suggestive of ‘‘molecular’’ states whose their structure is determined by the strong interaction dynamics

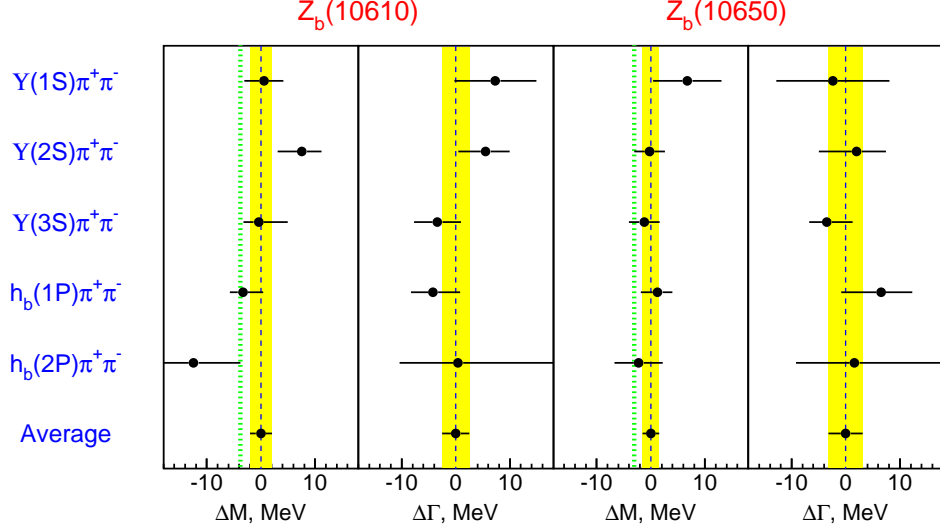


FIG. 11: Comparison of $Z_b(10610)$ and $Z_b(10650)$ parameters obtained from different decay channels. The vertical dotted lines indicate $B^*\bar{B}$ and $B^*\bar{B}^*$ thresholds.

of $B^*\bar{B}$ and $B^*\bar{B}^*$ meson pairs.

The widths of both states are similar and are of the order of $15 \text{ MeV}/c^2$. The $Z_b(10610)$ production rate is similar to the $Z_b(10650)$ production rate for every decay channel. Their relative phase is consistent with zero for the final states with the $\Upsilon(nS)$ and consistent with 180 degrees for the final states with $h_b(mP)$.

The $\Upsilon(5S) \rightarrow h_b(mP)\pi^+\pi^-$ decays seem to be saturated by the $Z_b(10610)$ and $Z_b(10650)$ intermediate states; this decay mechanism is responsible for the high rate of the $\Upsilon(5S) \rightarrow h_b(mP)\pi^+\pi^-$ process measured recently by the Belle Collaboration.

Analysis of angular distributions for charged pions favors the $J^P = 1^+$ spin-parity assignment for both $Z_b(10610)$ and $Z_b(10650)$. Since the $\Upsilon(5S)$ has negative G-parity, Z_b states will have opposite G-parity due to emission of the pion.

ACKNOWLEDGEMENT

We are grateful to Alexander Milstein of BINP and Mikhail Voloshin of the University of Minnesota for fruitful discussions.

We thank the KEKB group for excellent operation of the accelerator, the KEK cryogenics group for efficient solenoid operations, and the KEK computer group and the NII for valuable computing and SINET4 network support. We acknowledge support from MEXT, JSPS and

Nagoya's TLPRC (Japan); ARC and DIISR (Australia); NSFC (China); MSMT (Czechia); DST (India); MEST, NRF, NSDC of KISTI, and WCU (Korea); MNiSW (Poland); MES and RFAAE (Russia); ARRS (Slovenia); SNSF (Switzerland); NSC and MOE (Taiwan); and DOE and NSF (USA).



- [1] K.-F. Chen *et al.* (Belle Collaboration), Phys. Rev. Lett. **100**, 112001 (2008).
- [2] I. Adachi *et al.* (Belle Collaboration), e-Print: arXiv:1103.3419 [hep-ex]
- [3] S. Kurokawa and E. Kikutani, Nucl. Instrum. Methods Phys. Res. Sect. A **499**, 1 (2003), and other papers included in this Volume.
- [4] A. Abashian *et al.* (Belle Collaboration), Nucl. Instrum. Methods Phys. Res., Sect. A **479**, 117 (2002).
- [5] R. Brun *et al.*, GEANT 3.21, CERN DD/EE/84-1, 1984.
- [6] K. Nakamura *et al.* (Particle Data Group), J. Phys. **G 37**, 075021 (2010).
- [7] T. Skwarnicki, Ph.D. Thesis, Institute for Nuclear Physics, Krakow 1986; DESY Internal Report, DESY F31-86-02 (1986).
- [8] S.M. Flatté, Phys. Lett. B **63**, 224, (1976).
- [9] A. Garmash *et al.* (Belle Collaboration), Phys. Rev. Lett. **96**, 251803 (2006).
- [10] M.B. Voloshin, Prog. Part. Nucl. Phys. **61**, 455 (2008).
M.B. Voloshin, Phys. Rev. D **74**, 054022 (2006).
- [11] G.C. Fox and S. Wolfram, Phys. Rev. Lett. **41**, 1581 (1978).
- [12] J. Blatt and V. Weisskopf, Theoretical Nuclear Physics, p.361, New York: John Wiley & Sons (1952).
- [13] The angular distributions for various J^P hypothesis of the Z_b were calculated by A. Milstein (private communications).
- [14] For the $Z_b(10610) \rightarrow \Upsilon(3S)\pi$ decay the pion from the $Y(5S)$ decay and the pion from the $Z_b(10610)$ decay have similar momenta and are difficult to distinguish. Therefore for $\cos\theta_1$ ($\cos\theta_2$) we use cosine of the π^+ (π^-) polar angle and we average the fit functions among $\cos\theta_1$ and $\cos\theta_2$.